A Fast Noise-Predictive Multiphysical Model of the PWM-controlled Induction Machine

J. Le Besnerais, A. Fasquelle, M. Hecquet, V. Lanfranchi, P. Brochet, and S. Bujacz

***Abstract*— a multi-physical parametric model of the induction machine and its pulse width modulation (PWM) supply was developed in order to predict its sound power level of electromagnetic origin at variable speed and load, and perform optimal design search including noise minimization. The electromagnetic model calculates the stator phase currents by the aid of a Simulink® PWM model and a multilayer single-phase equivalent circuit; it computes the air-gap radial flux density which is supposed to be the only source of acoustic noise. The mechanical and acoustic parts are based on a 2D cylindrical shell stator model.**

This paper presents some variable-speed simulations of a squirrel-cage traction machine, and demonstrates the ability of the simulation tool to investigate the role of harmonics in noise generation. Then, the possibility to use the Design of Experiments (DoE) method in order to find the leading variables on noise at variable speed is discussed. Finally, some PWM simulation results are presented and interpreted on the base of theoretical results.

***Index Terms*—magnetic noise, induction machine, PWM strategies, experimental designs.**

I. Introduction

As progress is being made in motor noise reduction of mechanical source (e.g. bearings) and aeraulic source (e.g. fans), the understanding and prediction of the noise of electromagnetic origin in adjustable-speed motors becomes crucial. In fact, the various PWM strategies used during traction and braking add significant harmonic contents to the air-gap Maxwell forces spectrum, leading to possibly harmful noise and vibrations. This so-called "magnetic noise" problem involves several domains of physics (electronics, electromagnetism, mechanics and acoustics): thus, only a global approach, integrating together the motor structure, its environment and its converter, can tackle it.

This paper presents a simulation tool of the PWM-fed induction machine, DIVA, which is able to consider the whole space and time harmonics involved in magnetic noise generation without a prohibitive computation time. In a first part are detailed the electromagnetic, mechanical and acoustic analytical models of DIVA [1] and their validation with FEM simulations or experiments. Secondly, some variable-speed simulation results are presented. In particular, a method for investigating the role of harmonics in magnetic noise generation is demonstrated. Then, some Designs of Experiments (DoE) are performed with respect to noise response, and the possibility to infer some conception rules of variable-speed quiet motors from these parametric studies is discussed. Finally, the simulated noise spectrum of a traction machine under synchronous strategy is presented and interpreted.

The motor studied in this paper is a 250 kW three-phase squirrel-cage induction machine with p=3 pole pairs, Z_R=28 rotor bars and Z_S=36 stator slots.

II. Electromagnetic Model

A. Supply voltage computation

The supply phase voltage can be either given by experimental data, computed analytically or with a Simulink® model. DIVA handles the main PWM strategies: asynchronous, synchronous, angle-calculated and full-wave. All these strategies are involved during traction and braking, and their design is based on many criteria (switching losses, harmonic elimination, thermal constraints and motor performances).

B. Currents computation

The stator and rotor phase currents are computed using an extension of the classical fundamental single-phase equivalent circuit (Fig. 1), including all space and time harmonics [2], and the skin effect modeling. The resolution of this multilayer circuit can be expressed in a matrix form and therefore be solved very quickly in Matlab®.

C. Magnetomotive forces and permeance computation

Many authors use the Fourier-expanded magnetomotive forces (mmf) and permeance functions in their model, which leads to complex expressions with multiple summations, large

Manuscript received June 30, 2006. This work was supported in part by the French Agence de l'Environnement et de la Maîtrise de l'Energie (ADEME).

J. Le Besnerais is with the Laboratoire d'Electrotechnique et d'Electronique de Puissance (L2EP), Ecole Centrale de Lille, 59 651 Villeneuve d'Ascq, FRANCE, (+33 (0)6 81 08 62 31; e-mail: jean.le_besnerais@centraliens.net). M. Hecquet, P. Brochet and S. Bujkaz are with the L2EP (e-mail: michel.hecquet@ec-lille.fr). A. Fasquelle is with the L2EP and the Laboratoire de Mécanique et d'Energétique (LME), 59313 Valencienne, FRANCE. V. Lanfranchi is with the Laboratoire d'Electromécanique de Compiègne (LEC), UTC, Compiègne, FRANCE..

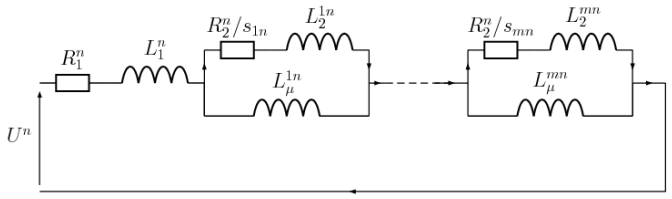

Fig. 1. Single phase equivalent circuit of the *n*-th time harmonic layer. U^n is the *n*-th component of the supply phase voltage spectrum at frequency f_n, and $s_{mn}=1-mf_0(1-s)/f_n$ stands for the harmonic slip of the *m*-th space harmonic and *n*-th time harmonic, *s* being the fundamental slip.

computation times and search of a compromise between simulation speed and precision. However, this approach helps to quantify the role of space and time harmonics in the magnetic noise generation process, and allows making a theoretical modal analysis before implementation. An other method consists in directly implementing these functions by the aid of the so-called *winding functions* [3] (WF), which allows not only to model any type of winding and cage without any symmetry hypothesis (e.g. fractional slot windings and broken bar cages), but also to achieve very fast simulation times. As DIVA aims at diagnosing magnetic noise real cases and performing global optimizations, it includes both methods.

The phase WFs are the phase mmf for a unit current, and they are characterized by:

$$f_{mm}^s(t,\alpha_s)=\sum_{q=1}^{q_s} i_q^s(t)WF_q(\alpha_s) \quad (1)$$

where f^s_{mm} is the total stator mmf, i^s_q is the *q*-th phase current, and α_s represents the stator fixed frame mechanical angle. The WFs linearly rise in the slots, and remain constant in the teeth. Their computation is based on the fact that a two-coil mmf can be decomposed into a sum of two functions (called elementary winding function, or EWF) weighted with opposite signs as showed in Fig. 2. In DIVA, the stator winding distribution is represented by a matrix M_w of size (q_s, Z_S) where q_s is the number of phases. This matrix contains the number of turns in series associated to each phase and slot, which is either positive or negative according to current direction. Each phase mmf is then computed as:

$$WF_q(\alpha_s)=\sum_{j=1}^{Z_s} M_w(q,j)EWF(\alpha_s,\alpha_j) \quad (2)$$

where α_j stands for the angular position of the *j*-th stator slot.

The typical shapes of a shorted-pitch motor WFs are represented in Fig. 3. The EWFs are used in a similar way for rotor mmf computation with some equivalent numbers of turns and phases (Fig. 4).

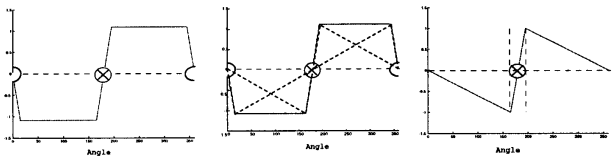

Fig. 2. Winding function (WF) of a two coils winding, equivalent winding functions distribution and elementary winding function (EWF) [2].

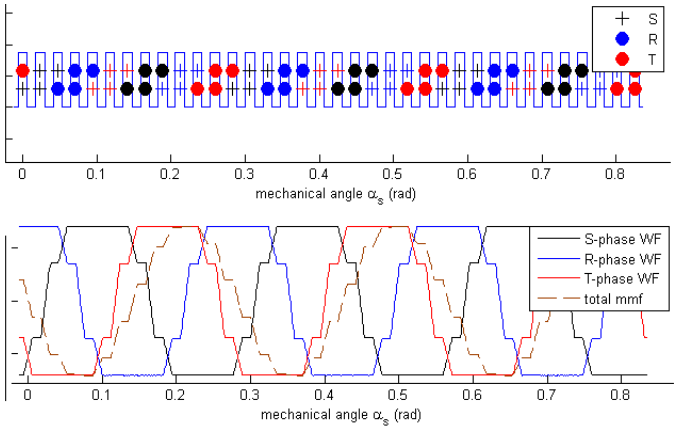

Fig. 3. Phase windings functions, total winding function and normalized total mmf of a shorted-pitch winding in function of stator mechanical angle.

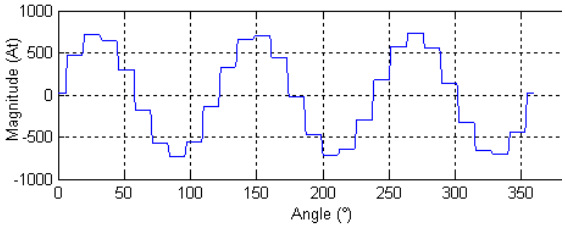

Fig. 4. Rotor mmf of 28 bars at a given time in function of mechanical angle.

D. *Air-gap radial force computation*

The radial air-gap induction B_g is expressed as

$$B_g(t,\alpha_s)=\Lambda(t,\alpha_s)(f_{mm}^s(t,\alpha_s)+f_{mm}^r(t,\alpha_s)) \quad (3)$$

where $\Lambda=\mu_0/g_e$ is the air-gap permeance per unit area, and g_e is the effective air-gap width: its value is either the air-gap width g, $g+p_S$, $g+p_R$, or $g+p_S+p_R$ whether two teeth face each other, a stator tooth faces a rotor slot, a rotor tooth faces a stator slot or two slots face each other respectively. The values of the fictitious stator and rotor slot depths p_R and p_S were taken as suggested by [4] proportionally to the rotor and stator slot openings (l_{RE}/5 and l_{SE}/5), which finally gave some good results.

E. *Skew modeling*

The skew effect is based on a multi-slice model. It consists in computing the air-gap induction B_{sk} in a series of n_{sk} motor slices rotated one from another of a skew angle fraction. The real air-gap induction is then simply computed as:

$$B_g=\sum_{i=1}^{n_{sk}} B_{sk}^i/n_{sk} \quad (4)$$

F. *Validation*

The radial air-gap induction compares very favorably with FEM simulations (FLUX2D®) for different machines, supply frequencies and voltages (Fig. 5), except in saturated regions which are not handled by DIVA yet. The shorted-pitch stator mmf was also successfully compared to FEM results.

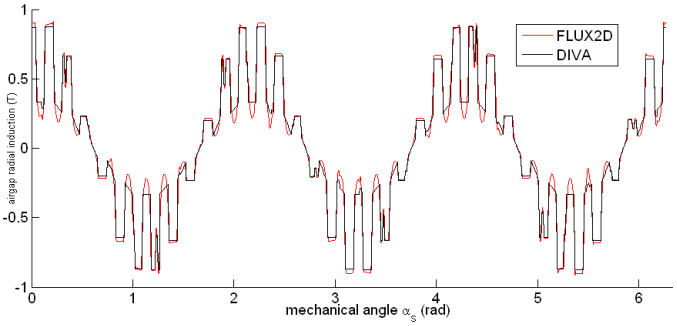

Fig. 5. FEM and DIVA air-gap radial induction as a function of stator mechanical angle under sinusoidal supply at f_0 = 50 Hz and U_0=173V (off-load case, s=0.01%).

The phase current was validated at various voltages with FEM and experiments in off-load and on-load cases (Fig. 6). The motor performances (power factor, electromagnetic torque and power, efficiency) in variable-speed have been also checked. All these quantities are computed in DIVA besides the noise level with a view to find the optimal design of the induction motor with several objectives.

The SQP local optimization method was used in order to compute the optimal skew factor of the rotor cage (Fig. 7). The well-known optimal skew angle of one slot pitch was found with a precision of 1% for n_{sk}=100, partly validating DIVA skew model.

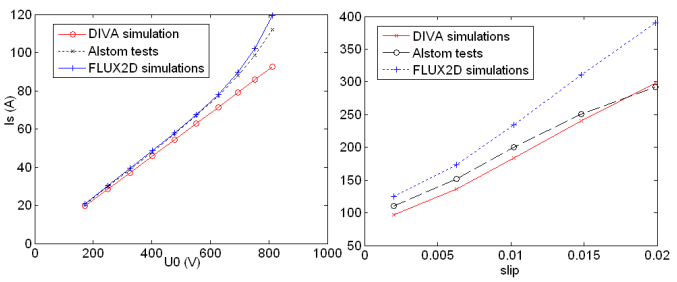

Fig. 6. DIVA, FLUX2D and experimental phase current in function of supply voltage in off-load case (left) and in function of slip (right) (sinusoidal case at f_0 = 50 Hz).

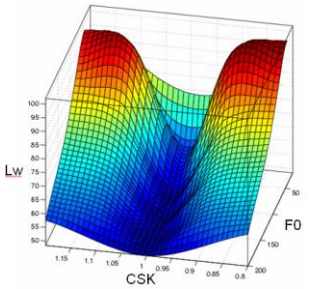

Fig. 7. Noise in function of rotor skew factor *CSK* (in stator slot pitch) and supply frequency. The minimum noise corresponds to 1 slot pitch at all frequencies.

III. Mechanical Model

A. Exciting force computation

Neglecting the tangential component of the Maxwell tensor and the magnetostriction effect, the exciting pressure F_r responsible for magnetic noise can be approximated by [5]:

$$F_r = B_g^2/(2\mu_0) \tag{5}$$

B. Speed vibration computation

The mechanical model assumes that the stator is a free-free 2D thin cylindrical shell. Therefore, only the circumferential spatial modes are considered. The static radial displacements Y_{sm} are first computed from the complex amplitudes F_{mw} of the 2D discrete Fourier transform (FFT2) of F_r. For mode numbers ≥ 2, they are given by

$$Y_{sm} = 12R_a R_m^{\,3} F_{mw}/(Eh^3(m^2-1)^2) \tag{6}$$

where h is the thickness of the stator back, R_m is the mean stator radius (computed without considering the teeth), E is the stator's Young modulus and R_a is the stator bore radius. Then, the dynamic displacements Y_{dm} are computed by the aid of a second order transfer function:

$$Y_{dm} = Y_{sm}\left[(1-f^2/f_m^{\,2})^2 + 4\zeta(f_m)^2 f^2/f_m^{\,2}\right]^{-1/2} \tag{7}$$

where ξ is the damping coefficient, and f_m is the m-th mode natural frequency. ξ is supposed to depend on the mode and its variation with frequency is modeled as in [6]. The natural frequencies are for m ≥ 2 [5]:

$$f_m = f_0 h\, m(m^2-1)/(2\sqrt{3}R_m\sqrt{m^2+1})$$
$$f_0 = \sqrt{E/(\Delta\rho)}/(2\pi R_m) \tag{8}$$

where f_0 is the zero mode natural frequency, ρ is the stator mass per unit volume, and Δ is a stator mass correction factor which includes the windings and teeth ones [1]. To consider the stator finite length effect, the first natural frequencies are multiplied by additional coefficients as explained in [2]. If the motor environment is suspected to greatly change the stator free-free natural frequencies, it is always possible to introduce in DIVA some more precise natural frequencies and damping coefficients computed with a complete FEM model of the motor's mounting and coupling.

C. Validation

The analytical natural frequencies prove to agree well with FEM simulations and impact testing measurements (Tab. 1).

Mode number	Analytical method natural frequency (Hz)	Experimental method natural frequencies (Hz) and damping coefficients (%)
0	3300	3283 (1.5)
2	688	616 (2.16) – 731 (2.22)
3	1775	1406 (1.47) – 1622 (2.1) – 1769 (1.16)
4	3340	3106 (0.96) – 3383 (0.88)

Tab. 1. Analytical and experimental natural frequencies of an induction machine stator.

IV. Thermal Model

An important factor involved in motor optimal design is temperature: hence, DIVA is being coupled with a nodal-network-based thermal model which has the specificity to be able to take into account the fluid flow within the motor, and thus to compute the air temperature. The main connection between DIVA and this thermal model is the electromagnetic losses computation [7].

V. Acoustic Model

A. Sound power level computation

The acoustic model computes the sound power radiated by each spatial mode

$$W_m(f) = \rho_0 c S \sigma_m(f) \left| 2\pi f Y_{dm} \right|^2 / 2 \quad (9)$$

where σ_m is the radiation factor, ρ_0 the air density, c the speed of sound and S the stator outer surface. The radiation factor computation is either based on its cylindrical or spherical approximation according to the motor shape [6]. The total sound power $W(f)$ is the sum of the sound power radiated by each mode. The total sound power level associated to a given frequency is then

$$L_w(f) = 20\log(W(f)/W_0), \quad (10)$$

with W_0=1 pW, and the total A-weighted sound power level is

$$L_{wA} = 10\log\left(\sum_f 10^{0.1 w_A(f) L_w(f)}\right) \quad (11)$$

where $w_A(f)$ stands for the A-weight at frequency f.

B. Validation

The sound power level of electromagnetic origin could not be experimentally validated as it is hard to separate it from the mechanical and aeraulic noise. However, the level of the simulated main slotting rays was found to be close from one of the experiments led on a water-cooled induction motor, and the main resonances are well predicted by DIVA [8]. Moreover, the same quietest combinations of Z_R and Z_S were found as reported in recent FEM simulations [9]: the noise level *trends* are respected, which is the most important for the optimization feature of DIVA.

VI. Simulation Results

A. Variable-speed noise spectra

Understanding which space or time harmonics contribute the most to a high magnetic noise level is essential in order to properly correct the motor design. Using DIVA, it is possible to study "virtual motors" with or without any type of harmonics, and then quantify the harmonics interactions and their contribution to each noise spectrum ray and each mode.

In this example, a simulation (Fig. 8) was run under sinusoidal supply in off-load case (s=0.01%), with a constant ratio U_0/f_0 until 138 Hz, and then a constant voltage U_0. Four machines were studied: the initial design (all harmonics), one without winding space harmonics, one without slot space harmonics, and one without any harmonics (fundamental).

The results agree well with Timar analytical work [6]. As expected, the winding and slot space harmonics increase the noise level (note that the effect of winding harmonics is underestimated as the studied motor is already shorted-pitch). However, in that case, the space harmonics that contribute the most to the global noise level are clearly the slotting ones.

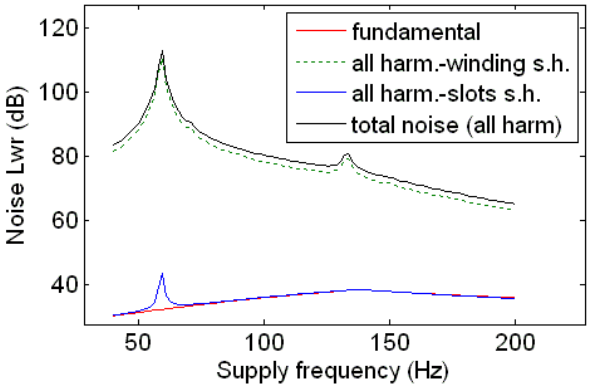

Fig. 8. Off-load sound power level in sinusoidal variable-speed case.

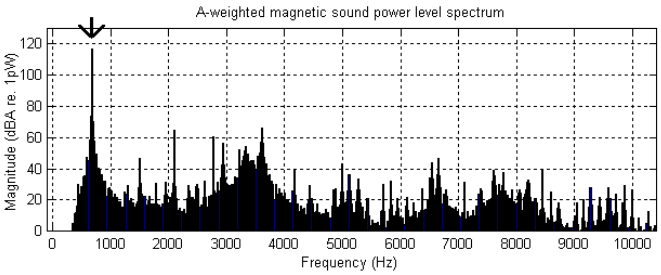

Fig. 9. A-weighted sound power level under sinusoidal supply in off-load case at f_0 = 60 Hz and U_0 = 300 V.

The resonance peak around 60 Hz results from the match between the exciting frequency $f_0((1\text{-}s)Z_R/p+2)$=680Hz (coming from the interaction between the fundamental current and the permeance waves harmonics) of mode number $Z_S\text{-}Z_R+2p$=2 and the second mode natural frequency at 688 Hz. This is a typical magnetic ray which generates a high tonal noise, as seen in the A-weighted sound spectrum (Fig. 9).

B. Computation time

In the worst case (on-load PWM supply with 200 time harmonics), the program runs in 6s for 1000 time-steps on a rotor rotation period and 1000 angular points on the stator circumference on a 2GHz laptop. The computational bottleneck is the rotor mmf computation, which requires computing the rotor currents in each bar at every time-step. In the best case (off-load sinusoidal supply), it takes less than 0.5s with the same precision. To compute the variable speed noise generation, these simulation times have to be multiplied by the number of speed points which has to be enough high to fully take into account the resonance effects. However, DIVA variable-speed simulation time is still enough low to be able to perform global optimizations.

VII. Design of Experiments

DIVA is coupled to a Design of Experiments software [10]. Here, this tool is used for its *screening* feature, i.e. its ability to analyze the leading design variables (or *factors*) on various *responses* such as magnetic noise, motor efficiency, etc, rather than for its optimization algorithm or its *response surfaces method* (RSM) feature. The screenings help to eliminate the

design variables the least influential on the objective functions before launching any optimal search, whereas the RSM aims at finding a polynomial approximation of the noise response in function of design variables. Such a relation would be a great advance in the electrical machines noise field as mentioned in [11].

The screening results are based on the response evaluation at two levels for each factor, and assume that the response behaves linearly between these bounds (in the following examples, these bounds are fixed taking ±5% of the tested motor parameters). Just like the RSM, the screenings cannot handle discrete factors. Consequently, the variables like p, Z_R, Z_S and the coil pitch cannot be considered in such studies. It happens that it is exactly p, Z_R and Z_S which characterize the most the exciting forces spectrum and modes, so the screenings will only be able to quantify the factors influence on noise through the stator structure modification and not the exciting forces modification. Furthermore, any polynomial approximation of the noise response found by the RSM will be inevitably specific to a given force distribution.

A first study, run under sinusoidal supply at various frequencies, shows unsurprisingly that among all the geometric design variables the leading ones on noise are h_{cul} (height of yoke), D_{sext} (stator outer diameter), *gap* (airgap width), l_{RE} and l_{SE} (slot openings) and the skew factor *pasv* (Fig. 10). More interestingly, h_{cul} turns out to be even more influent than *pasv* at certain frequencies. Likewise, the factors D_{sext} and h_{cul} have opposite influences in function of the speed. For instance, a h_{cul} increase lowers the noise level at f_0=50 Hz and increases it at f_0=70 Hz (Fig. 11). In fact, at a given supply frequency, the best design will be the one which puts its natural frequencies the furthest away from the corresponding exciting force frequencies: it can therefore greatly change with speed. In this example, the main force excites the stator second mode of frequency 688 Hz at f_{exc}=565 Hz for f_0=50 Hz and at f_{exc}=792 Hz for f_0=70 Hz: therefore, as the natural frequency of mode 2 increases with h_{cul} but decreases with D_{sext} (8), a h_{cul} increase reduces the noise at f_0=50 Hz, but increases it at f_0=70 Hz because it brings the natural frequency closer to the exciting force frequency. Moreover, the effect of h_{cul} is larger at 50 Hz than at 70 Hz because f_{exc}=792 Hz is closer from 688 Hz.

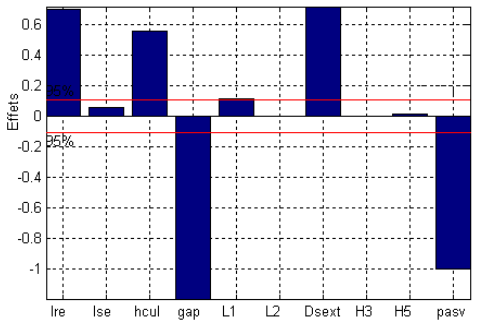

Fig. 10. Relative effects of 10 design variables on noise (*screening*) under sinusoidal supply at f_0 = 90 Hz. *L1*, *L2*, *H3* and *H5* are respectively the stator and rotor stack lengths and slot depths. The horizontal line is the user-defined significance threshold. A positive level indicates that the factor and the response increase together.

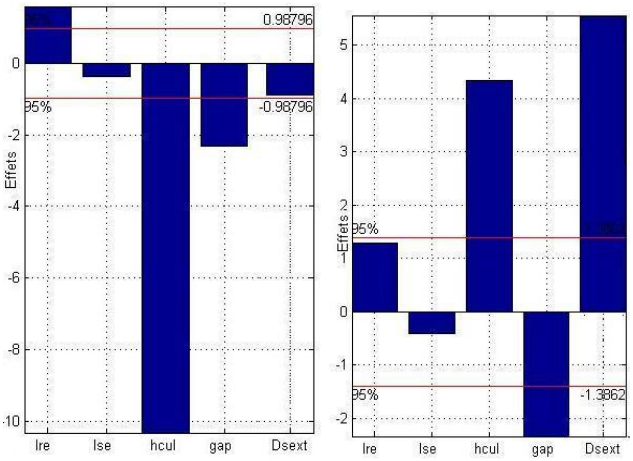

Fig. 11. Relative effects of 5 design variables on noise (*screening*) under sinusoidal supply at f_0 = 50 Hz (left) and 70 Hz (right).

The other factors have the same influence over the whole speed range, and the following passed conclusions were drawn again: when significant, a l_{RE} or l_{SE} increase raises the noise, whereas a *gap* or *pasv* increase lowers it (except when skewing the rotor above the optimal skew factor of one stator slot pitch, which increases the noise level cf. Fig. 7).

This example underlines the importance to define a noise response function independent of the speed in order to be able to infer some reliable conception rules of variable-speed motors. One can use for instance the speed-averaged noise level (noted L_{w1}), but not the maximum noise level encountered in the whole speed range (L_{w2}), as it would bring the same problems as previously pointed up (for instance, the results would depend on whether f_{exc}>688 Hz or f_{exc}<688 Hz i.e. especially on the speed discretization step). The screening results with L_{w1} and L_{w2} are presented in Fig. 12. Considering the average noise, the last conclusions are found again for l_{RE}, l_{SE} and *gap*. However, for this specific example, the influence of D_{sext} and h_{cul} are rather counter-intuitive: *generally*, the more compact (low D_{sext}) and thick (high h_{cul}) a motor, the quieter… Here, the screening results give rise to a model which is actually noisier far from resonances, but quieter at resonances, and globally with a lower speed-averaged noise L_{w1}.

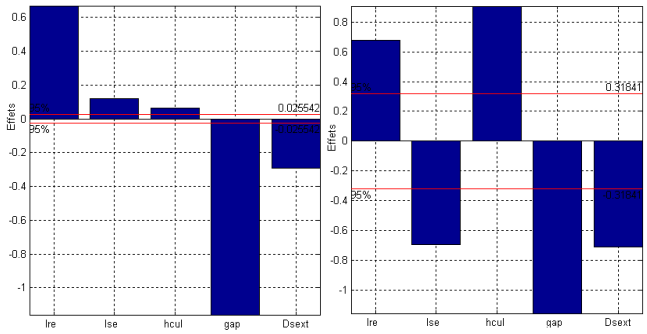

Fig. 12. Relative effects of 5 design variables on noise (*screening*) under sinusoidal supply at variable speed, for noise response L_{w1} (left) and L_{w2} (right).

VIII. PWM Simulations

In Fig. 13 are compared the noise spectra obtained at f_0 = 40 Hz, U_0 = 300 V under sinusoidal supply and under PWM supply (synchronous mode, switching frequency f_s = 840 Hz). With the ideal supply, the highest ray is due to the previous slotting resonance at $f_0((1\text{-}s)Z_R/p+2)$=450 Hz. In the PWM case, this ray still exists with the same amplitude. This illustrates the fact that a noisy motor will remain noisy with a PWM inverter. However, many new rays appear [12], like the one at 720 Hz. By analyzing the radial force FFT2 plot in DIVA, one can easily observe that the main PWM harmonic forces have a 0 or 2p mode order, and that this resonance peak is produced by a large zero-mode force ray at 720 Hz. In fact, it is possible to analytically find that this ray comes from the interaction between the supply current fundamental and the PWM harmonics, and that its frequency is precisely $(f_s\text{-}4f_0)+f_0$ =720 Hz [13]. The highest ray occurs at 3360 Hz, it results from the constructive interference between a slotting ray of mode number $9Z_R\text{-}7Z_S$=0 and frequency $f_0(9(1\text{-}s)Z_R/p)$= 3359.7 Hz, and a PWM ray of mode number $2p$=6 and frequency $(5f_s\text{-}20f_0)\text{-}f_0$ =3360 Hz.

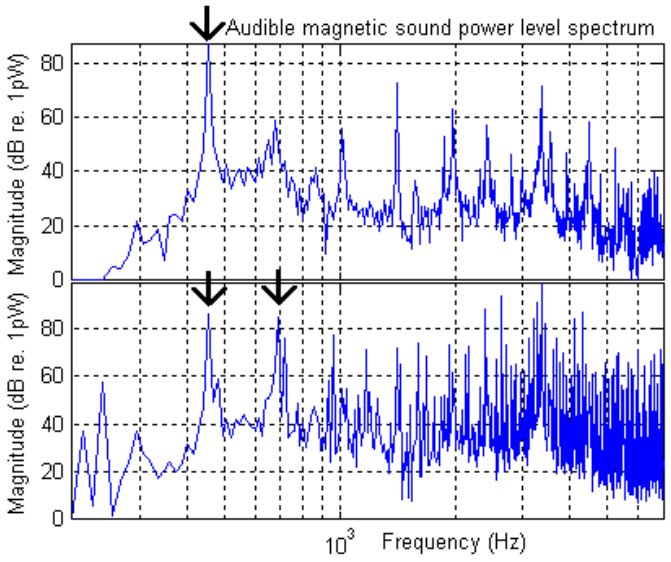

Fig. 13. Sound power level spectra under sinusoidal supply (up) and synchronous PWM supply at 840 Hz switching frequency (down) in off-load case at f_0 = 40 Hz and U_0 = 300 V.

IX. Conclusion

DIVA is a powerful simulation tool for electromagnetic noise prediction and diagnostic of variable-speed motors. The simulation results match very well with experiments in non-saturated and sinusoidal case, and the simulation results have been successfully interpreted with the theory of electromagnetic noise generation in both sinusoidal and PWM cases.

If it is illusory to search a polynomial approximation of the noise response even in function of the main design variables, the example of DIVA proves that some fast and reliable analytical tools can be developed in order to carry out parametric studies and global optimizations. In addition, it has been shown how the screening results have to be interpreted with much caution, as they highly depend on the definition of the global noise response function.

Future work will validate the PWM results with experiments and FEM simulations, prospect the acoustic behaviour of various supply strategies, and deal with the global optimization of the PWM-fed induction machine with respect to noise level, efficiency, temperature, core losses and material cost. The acoustic model will be also improved in order to take into account longitudinal modes as well as different boundary conditions. Finally, the saturation effect should be considered in the electromagnetic model and its consequences on noise should be investigated.

References

[1] A. Ait-Hammouda, “Prédimensionnement et étude de sensibilité vibro-acoustique de machines à courant alternatif et à vitesse variable” Ph.D. dissertation, USTL, Lille, FRANCE, 2005.

[2] A. Hubert, “Contribution à l’étude des bruits acoustiques générés lors de l’association machines électriques - convertisseurs statiques de puissance. Application à la machine asynchrone” Ph.D. dissertation, Université des Technologies de Compiègne, FRANCE, 2000.

[3] A. Ghoggal, M. Sahraoui, A. Aboubou, S.E. Zouzou and H. Razik, “An improved model of the induction machine dedicated to faults detection – extension of the modified winding function approach,” in *ICIT 2005 IEEE Int. Conf. on Industrial Technology*, pp. 191–196.

[4] J. F. Brudny, “Modélisation de la denture des machines asynchrones : phénomènes de résonances,” *J. Phys. III*, vol. 37, no. 7, 1997.

[5] Kelvin C. Maliti, “Modelling and analysis of magnetic noise in squirrel-cage induction motors,” Ph.D. dissertation, Royal Institute of Technology, Dpt. of Electric Power Engineering, Stokholm, SWEDEN, 2000.

[6] P. L. Timar, “Acoustic noise of electromagnetic origin in an ideal frequency-converter-driven induction motor,” *IEE Proc. on Elec. Power Appl.*, vol. 141, no. 6, Nov. 1994.

[7] A. Fasquelle, A. Ansel, S. Brisset, P. Borchet and A. Randria, “Iron losses distribution in a railway traction induction motor,” *ICEM*, 2006.

[8] A. Ait-Hammouda, M. Hecquet, M. Gueygou, P. Brochet and A. RAndria “Prediction of the electromagnetic noise of an asynchronous machine using experimental designs,” *Mathematics and Computers in Simulation*, Elsevier, 2006, Vol. 71, issues 4-6, pages 409-419.

[9] I. Hirotsuka, K. Tsuboi and F. Ishibashi, “Effet of slot-combination on electromagnetic vibration of squirrel-cage induction motor under loaded condition,” *Proceedings of Power Conversion Conference*, Nagaoka, 1997.

[10] S. Vivier, A. Ait-Hammouda, M. Hecquet, B. Napame, P. Brochet and A. Randria, “Vibro-acoustic optimization of the permanent magnet synchronous machine using the experimental design method,” *Springer Monograph Recent Developments of Electrical Drives* (ICEM 2004), pp 101-114, 2006.

[11] P. Vijayraghavan and R. Krishnan, “Noise in electric machines: a review,” *IEEE Trans. on Ind. Appl.*, vol. 35, no. 5, Sept./Oct. 1999.

[12] V. Lanfranchi, A. Hubert and G. Friedrich, “Comparison of a natural sampling and a random PWM control strategy for reducing acoustic annoyances,” *European Power Electronics and drive conference (EPE’03)*, Toulouse, FRANCE, Sept. 2003.

[13] W. C. Lo, C. C. Chan, Z. Q. Zhu, L. Xu, D. Howe and K. T. Chau, “Acoustic noise radiated by PWM-controlled induction machine drives,” *IEEE Trans. on Ind. Elec.*, vol. 47, no. 4, Aug. 2000.

[14] Y. Okuyama and S. Moriyasu, “Electromagnetic noise of induction motors driven by PWM inverters,” *Electrical Engineering in Japan*, vol. 133, no. 3, 2000.

[15] S. P. Verma and A. Balan, “Experimental investigations on the stators of electrical machines in relation to vibration and noise problems,” *IEE Proc. on Elec. Power Appl.*, vol. 145, no. 5, 1998.

[16] J. Le Besnerais, A. Fasquelle, M. Hecquet, V. Lanfranchi, P. Brochet, A. Randria, D. Zorzynski and S. Bujacz, ”A Fast Noise-Predictive Multiphysical Model of the PWM-controlled Induction Machine”, *ICEM 2006*.